Theoretical Analysis of Torque Performance of Magnetorheological Damper Using Herschel-bulkley Model

Shuangshuang Su, Xin Wang, Daoxuan Peng and Qing Ouyang *

College of Mechanical and Electrical Engineering, Jiaxing University, Jiaxing, 314033 China
* Corresponding author

Abstract: The application of rotary magnetorheological (MR) dampers, which can provide continuous controllable torque, gradually develops towards the trend of high rotate speed and high transfer torque. The Herschel-Bulkley constitutive model can describe the fluid shear thinning phenomenon and is widely used in high shear rate occasions. The parameters k and n in Herschel-Bulkley model, proved to be related to magnetic field strength, are the foundation and key to establish the torque model of MR device. In this paper, the torque model of multistage MR damper was established, and the model parameters were selected according to the results of magnetic field analysis. The influence of different model parameters on the device torque was obtained based on the theoretical analysis. The theoretical torque results are basically positively correlated with the current. The theoretical torque deviation at different currents and rotate speeds, especially in the case of low currents and speeds, which is mainly due to the mismatching of model parameters and the limitations of the structural design of MR device.

Keywords: rotary magnetorheological damper; Herschel–Bulkley model; torque model; magnetic field analysis

1. Introduction

Compared with linear magnetorheological (MR) damper, due to some advantages like small, compact structure, and good flow sealing effect, the rotary MR damper is especially suitable for rotate conditions, such as medical rehabilitation machine system [1,2], transmission mechanism [3,4] and torsional vibration control system [5,6], which require the damper to be able to rotate continuously and provide controllable damping torque.

At present, the research on the mechanical modeling of MR damper mainly focuses on the linear MR damper [7,8], while the rotary MR damper's modeling research is relatively few. As far as we know, no rotary MR damper model based on the Bingham plastic model, which is the most popular model for MR fluid, has been developed before 2008 [9]. Although the Bingham model is widely used in the modeling of rotary MR devices due to its simple form and clear concept, it cannot describe the dynamic characteristics of MR devices accurately. Specifically, the rotary MR damper usually works at a high speed, and the fluid bears a large shear rate, which results in "shear thinning phenomenon" [10] that cannot be described by Bingham model.

Farjoud *et al.* [11] verified the shear thinning characteristics of MR fluid under high shear rate through experiments, and proposed to use the Herschel-Bulkley model to more accurately reflect the shear thinning phenomenon of fluid viscosity. Similar studies on Herschel-Bulkley model in rotary MR damper also have been reported by other works [12-14]. Although the Herschel-Bulkley model is more accurate than the Bingham plastic model at high shear rates, the Herschel-Bulkley model requires more parameters and lacks experimental data of relevant parameters [11,15].

To solve this problem, Becnel *et al.* [16] established a magnetorheometer set-up and obtained the Herschel-Bulkley model parameters k and n of MRF-132 DG MR fluid under different magnetic fields. This model is applied to the torque analysis of the developed multistage rotary MR damper and its validity is verified. Specifically, we designed a rotary MR damper with four-stage parallel coil structure, and established a device's torque model based on Herschel–Bulkley constitutive model. The effects of different model parameters on the output torque of the MR damper were discussed, and the MR device's torque was calculated according to the model parameter values obtained in reference [16].

2. Multistage Rotary MR Damper Structure

The rotary type MR damper with multi-stage coil structure was designed and studied its mechanical properties by our research group [17]. The device contains four-stage parallel coils, magnetic conducting components (45# steel), rotate shaft (45# steel), cylinder component (aluminum), rolling bearings and coil frameworks (fluorine plastic), which is shown in Figure 1. A ring shear channel filled with MR fluid (Lord MRF-132 DG), is formed among the rotate shaft, the magnetic conducting component and the multi-stage coil. The MR fluid acts as a medium for torque transmission between the rotate shaft and cylinder component. The magnetic field lines pass through the annular magnetic conducting

parts, rotate shaft and the fluid channel, and form a magnetic loop around the coils. The magnetic field intensity in the fluid channel can be controlled by the coil's input current, thus determining the torque transmission capacity of the device. A separation layer is set between rolling bearing and the fluid cavity to prevent ferromagnetic particles in the MR fluid from entering the bearing and affecting the smooth rotation of the bearing. The structural parameters of the designed MR device are shown in Table 1.

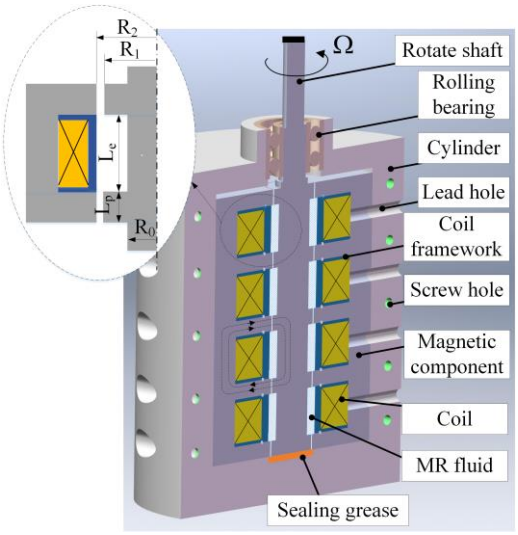

Figure 1. Schematic diagram of multistage rotary MR device structure.

Table 1. Structural parameters of designed MR damper.

R_0/mm	R_1/mm	R_2/mm	L_p/mm	L_e/mm	Turns of each coil N_T	Coil diameter d_c/mm
7	8.3	9.3	5	15	190	0.67

3. Magnetic Field Analysis

To obtain the magnetic induction intensity distribution in the fluid channel under different current conditions and verify the effectiveness of the magnetic circuit of the device, the magnetic field analysis was carried out by COMSOL Multiphysics analysis software.

The magnetic properties of the fluid are given by the manufacturer, and they are characterized by a yield stress-magnetic field strength relationship and a magnetization (B-H) curve. The relationship between the yield stress of fluid and magnetic field strength is shown in Figure 2(a). Furthermore, the B-H curve of the MR fluid and 45# steel are plotted in a logarithmic axis in Figure 2(b).

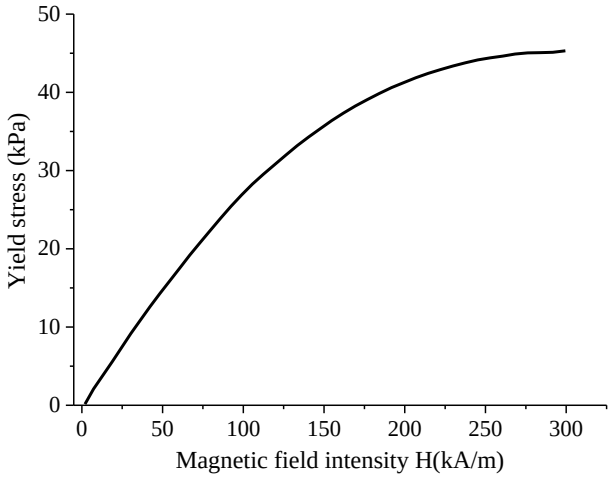

(a) Yield stress versus magnetic field strength

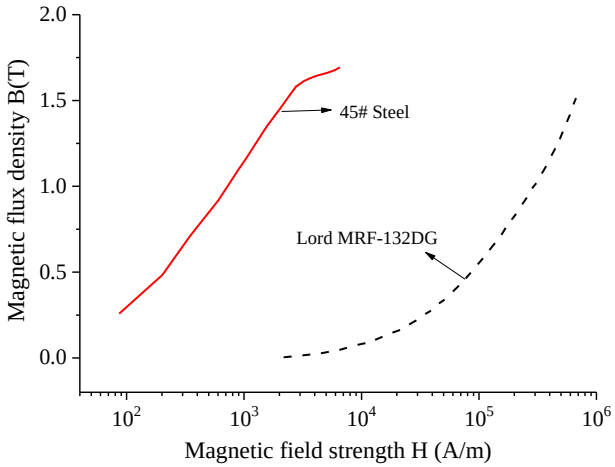

(b) Magnetization curves

Figure 2. Magnetic properties of MR fluid and 45# steel.

The yield stress of the MR fluid can be expressed as a cubic polynomial equation about the magnetic field intensity by using the numerical fitting method:

$$\tau_y = 4.141\times10^{-7}H^3 - 7.842\times10^{-4}H^2 + 0.351H - 0.704 \quad (1)$$

$$B = 1.321\times10^{-8}H^3 - 1.555\times10^{-5}H^2 + 7.27\times10^{-3}H + 1.188\times10^{-1} \quad (2)$$

Here, the units of yield stress and magnetic field strength is kPa and kA/m, respectively.

Using COMSOL's 2-D axisymmetric space to simplify the magnetic field analysis model. The model is subdivided by free triangular mesh. Taking 1 A current as an example, the magnetic field distribution and magnetic field line vector in the device are shown in Figure 3. The magnetic field lines in the effective annular fluid region generated by adjacent coils are in the same direction, vertically passing through the fluid channel and passing through the peripheral magnetic components to form a loop. The magnetic field can be ignored in the viscous annular shear region.

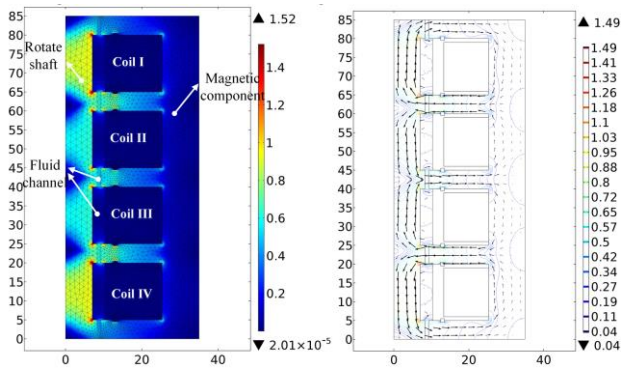

Figure 3. Magnetic field distribution (on the left) and magnetic field line vector (on the right)

The axial distribution (Z-axis) of magnetic induction intensity in the fluid channel under different input currents was analyzed, as shown in Figure 4. When the current increases from 0.5 A to 3.5 A, the magnetic induction intensity in the fluid channel increases and gradually becomes saturated. The magnetic induction intensity is distributed symmetrically in the axial direction, due to the geometrical symmetry of the MR damper and the consistency of material parameters of each coil and component, without considering magnetic flux leakage factor. It can also be seen from the Figure 4 that the magnetic induction intensity varies in different regions, which also increases the complexity of subsequent torque modeling.

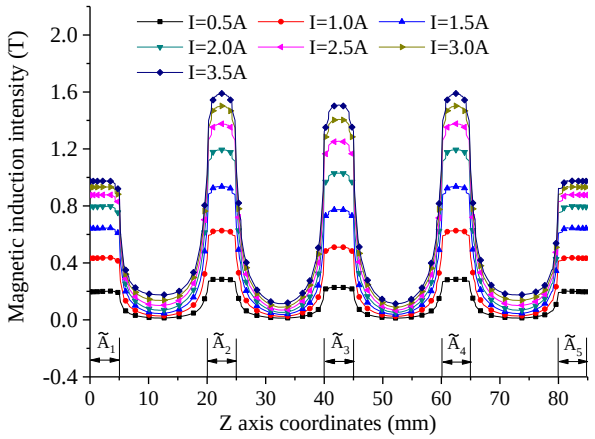

Figure 4. Distribution of magnetic induction intensity along the Z-axis.

According to Figure 4 and equations (1) ~ (2), the yield stress of different effective region under each current can be obtained. Figure 5 shows the relationship between the yield stress of MR fluid in each effective region and the input current. Due to the symmetrical distribution of the magnetic field of the device, the input current-yield stress curves basically coincide in regions $\widetilde{A}_1$ and $\widetilde{A}_5$, $\widetilde{A}_2$ and $\widetilde{A}_4$. It can be seen from the Figure 5 that when the input current reaches 2.5 A, the MR fluid in each region basically reaches the yield state, which can make the device exert greater controllability between 0 A to 2.5 A current.

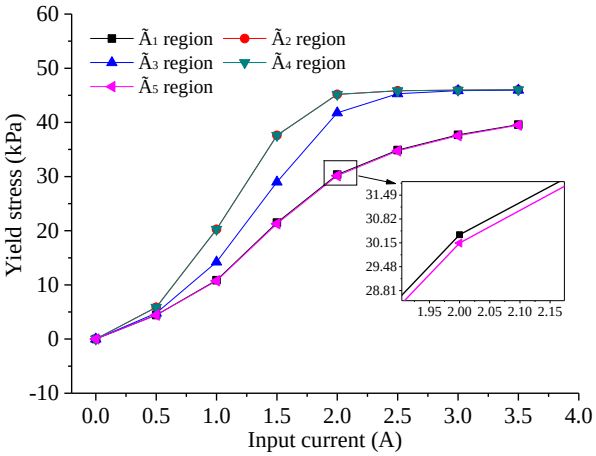

Figure 5. Input current-yield stress curves.

4. Torque Model Analysis

The shear stress of the MR fluid is provided by two parts: one is the effective annular shear region $\widetilde{A}$ vertically penetrated by the magnetic field, which is composed of five subregions: $\widetilde{A}_1$ ~$\widetilde{A}_5$; The second is the viscous annular shear region $\widetilde{B}$, which has a negligible magnetic field and is mainly composed of four subregions: $\widetilde{B}_1$~$\widetilde{B}_4$, as shown in Figure 6. The fluid in the effective annular shear region provides the coulomb torque produced by the magnetic field, and the viscous annular shear region provides the viscous torque caused by the fluid shear. In summary, the total torque was converted from the shear forces in these two regions.

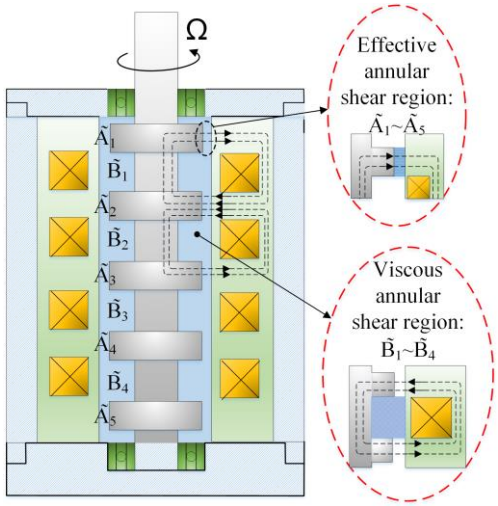

Figure 6. Schematic diagram of shear regions.

4.1. Torque Model of Effective Annular Shear Region

The torque model was established by taking the fluid in subregion $\widetilde{A}_1$ as an example. The inner and outer wall radii of the fluid in this region were R_1 and R_2 respectively, and its effective length was L_p. When the geometric size of the annular shear channel is small, the fluid in the area can be approximately considered to be in the stage of complete yield. Therefore, the shear strain rate $\dot{\gamma}$ of the fluid can be approximated as:

$$\dot{\gamma}_{A1}=\frac{2\pi}{60}\cdot\frac{R_2^2+R_1^2}{R_2^2-R_1^2}\Omega=\frac{\pi}{30}\cdot\frac{R_2^2+R_1^2}{R_2^2-R_1^2}\Omega \tag{3}$$

Here, Ω is rotate speed of shaft.

The relation between the fluid shear stress τ_{A1} and the torque T_{A1}^* can be expressed as [18]:

$$\tau_{A1}=\frac{T^*_{A1}}{2\pi L_p r^2}\quad (R_1<r<R_2) \tag{4}$$

From equation (4), it can be seen that the shear stress of the fluid is independent of the material properties, but related to the geometric parameters of the fluid shear channel. According to Mooney's hypothesis [19], the simplified shear stress of the fluid in the annular channel as follows:

$$\bar{\tau}_{A1}=\frac{1}{2}\left(\tau_{A1}\big|_{r=R_1}+\tau_{A1}\big|_{r=R_2}\right)=\frac{(R_1^2+R_2^2)}{4\pi L_p R_1^2 R_2^2}T^*_{A1} \tag{5}$$

Combined with Herschel-Bulkley model of MR fluid, the equation (5) can be further expressed as:

$$\bar{\tau}_{A1}=\tau_{yA1}+k\dot{\gamma}^n=\frac{(R_1^2+R_2^2)}{4\pi L_p R_1^2 R_2^2}T^*_{A1} \tag{6}$$

Here, τ_{yA1} is the shear yield stress provided by region $\widetilde{A}_1$, which is related to the magnetic field strength in this region. The exponent, *n*, is called the flow behavior index, and *k* is called the consistency parameter.

Substituting equation (3) into equation (6), the radius-related torque $T^*_{A1}(r)$ is transformed into the following form:

$$T_{A1}=\frac{4\pi L_p R_1^2 R_2^2}{(R_1^2+R_2^2)}\left\{\tau_{yA1}+k\left[\frac{\pi\Omega}{30}\cdot\left(\frac{R_2^2+R_1^2}{R_2^2-R_1^2}\right)\right]^n\right\} \tag{7}$$

where T_{A1} is the torque provided by the effective annular shear region $\widetilde{A}_1$, which is correlated with the geometry parameters of fluid channel, magnetic field strength, rotate speed, and the flow parameters *k* and *n*. It is assumed that the flow parameters *k* and *n* of each region are the same.

The torque provided by effective annular shear region $\widetilde{A}$ is the sum of the torque came from subregions $\widetilde{A}_1$ to $\widetilde{A}_5$. The geometric parameters of each subregion are the same, while the magnetic field intensity in the regions are different due to the magnetic field coupling effect of multi-stage coils. Therefore, the total torque in the effective annular shear region can be written as:

$$T_A=\frac{4\pi L_p R_1^2 R_2^2}{(R_1^2+R_2^2)}\left\{\sum_{j=1}^{5}\tau_{yAj}+k\left[\frac{\pi\Omega}{30}\cdot\left(\frac{R_2^2+R_1^2}{R_2^2-R_1^2}\right)\right]^n\right\} \tag{8}$$

where τ_{yAj} is the yield stress of the MR fluid in the j^{th} subregion $\widetilde{A}_j$.

4.2. Torque Model of Viscous Annular Shear Region

Taking the fluid in subregion $\widetilde{B}_1$ as an example, the inner and outer wall radii of the fluid in this region were R_0 and R_2 respectively, and its effective length was L_e. The angular velocity of the fluid in this region can be expressed as:

$$\omega(r)=\frac{R_0^2R_2^2}{R_2^2-R_0^2}\left(\frac{1}{r^2}-\frac{1}{R_2^2}\right)\cdot\frac{\pi}{30}\Omega \tag{9}$$

The radial distribution of the shear strain rate of the fluid is further deduced:

$$\dot{\gamma}_{B1}=-r\cdot\frac{d\omega}{dr}=\frac{\pi}{15\cdot r^2}\left(\frac{R_0^2R_2^2}{R_2^2-R_0^2}\right)\Omega \tag{10}$$

The torque generated by the fluid in region $\widetilde{B}_1$ is:

$$T_{B1}=\int_{R_0}^{R_2}2\pi r^2L_e\tau_{B1}dr=\int_{R_0}^{R_2}2\pi r^2L_e(k\dot{\gamma}_{B1}^n)dr \tag{11}$$

By substituting equation (10) into equation (11), the torque expression of region $\widetilde{B}_1$ can be obtained:

$$\begin{aligned}T_{B1}&=2\pi L_e k\left[\frac{\pi\Omega R_0^2R_2^2}{15(R_2^2-R_0^2)}\right]^n\cdot\int_{R_0}^{R_2}r^{(2-2n)}dr\\&=\frac{2\pi L_e k}{3-2n}\cdot\left[\frac{\pi\Omega R_0^2R_2^2}{15(R_2^2-R_0^2)}\right]^n\cdot\left(R_2^{3-2n}-R_0^{3-2n}\right)\end{aligned} \tag{12}$$

Similarly, the torque in the viscous annular shear region is the sum of the viscous torques in each shear subregion $\widetilde{B}_1$~$\widetilde{B}_4$, as shown in the following formula:

$$T_B=\frac{8\pi L_e k}{3-2n}\cdot\left[\frac{\pi\Omega R_0^2R_2^2}{15(R_2^2-R_0^2)}\right]^n\cdot\left(R_2^{3-2n}-R_0^{3-2n}\right) \tag{13}$$

According to equations (8) and (13), the total torque of the MR device can be obtained as follows:

$$T=T_A+T_B \tag{14}$$

5. Torque Evaluation and Analysis

5.1. Influence of Flow Characteristic Index

The damper torque is related to the flow characteristic index *k* and *n*. Figure 7 shows the theoretical torque changes with the different consistency parameters *k* at zero magnetic field when the flow index *n* = 1. The torque increases linearly with the rotate speed, and the greater the consistency parameters *k* is, the greater the torque will be. In view of Figure 7 (a), (b), it can be seen that that torque provided by the effective annular shear region $\widetilde{A}$ is much great than the torque of the viscous annular shear region $\widetilde{B}$ at the same flow parameters and the same rotate speed. As the coils are energized, this phenomenon will be more salient, that is, the torque provided by the effective annular shear region accounts for the majority of the total torque, it can also be shown in Figure 8.

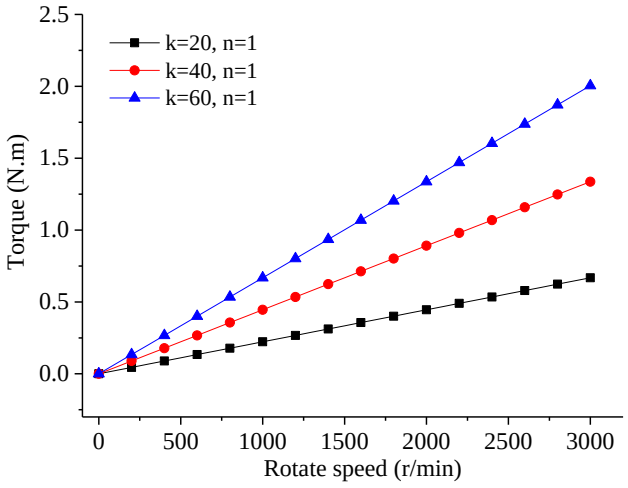

(a) Theoretical torques in the effective annular shear region

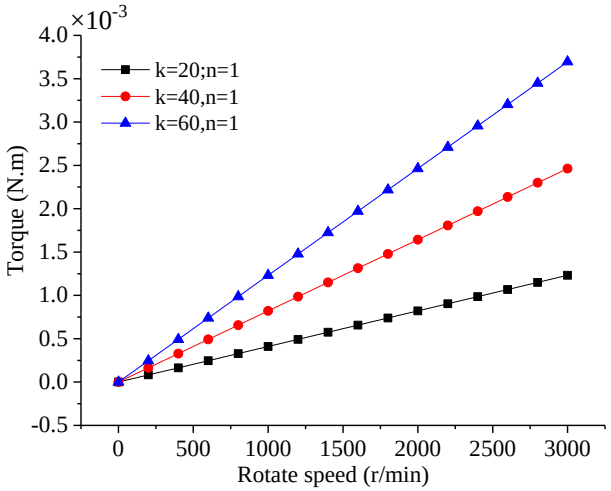

(b) Theoretical torques in the viscous annular shear region

Figure 7. Theoretical torque changes with the rotate speed at different k (n=1)

Figure 8 shows the variation law of theoretical torques in the two shear regions with rotate speed under different flow behavior index n (n<1) when the magnetic field is zero and k=40. When n is smaller, the shear thinning phenomenon of MR fluid is more significant, and the attenuation degree of provided torque is also greater at a certain speed. When the rotate speed is 3000 r/min and the flow index n is 0.6, 0.7 and 0.8, the corresponding torques are 0.056 N.m, 0.124 N.m and 0.274 N.m, respectively. When n=0.6, the attenuation amplitude of its torque is 54.93% and 79.65%, respectively, compared with that when n=0.7 and n=0.8. Therefore, the total torque of the MR damper can be approximately simplified to the torque provided by the effective annular shear region T_A.

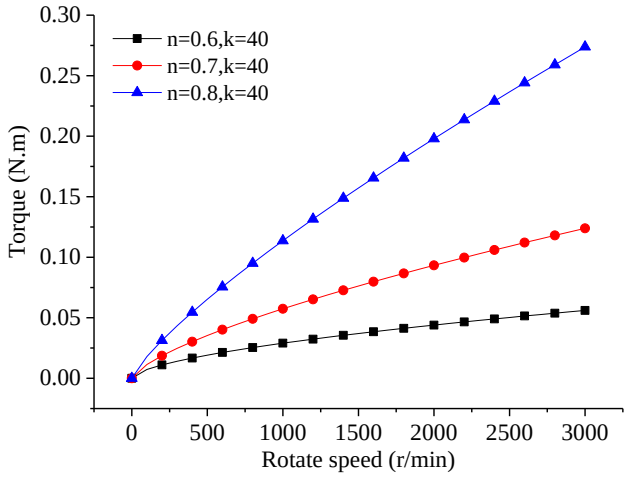

(a) Theoretical torques in the effective annular shear region

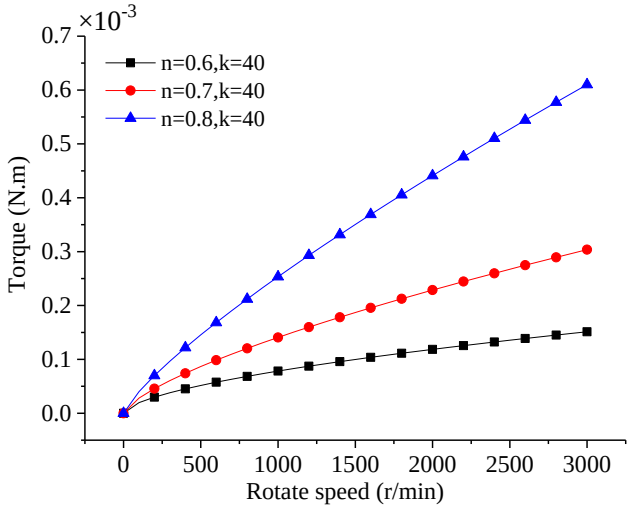

(b) Theoretical torques in the viscous annular shear region

Figure 8. Theoretical torque changes with the rotate speed at different n (k=40)

5.2. Theoretical Torque Analysis

The flow parameters k and n of Herschel-Bulkley are related to the magnetic field, specifically, the parameter k increases monotonously with the magnetic field strengths, and the parameter n decreases monotonously with the magnetic field strengths [16]. Here, the flow parameters k and n in each effective annular shear region ($\widetilde{A}_1$-$\widetilde{A}_5$) at different currents are shown in Table 2.

Table 2. Flow parameters in each effective annular shear region at different currents.

Shear region	Flow parameters	0.5 A	1.0 A	1.5 A	2.0 A
$\widetilde{A}_1/\widetilde{A}_5$	τ_{yAj} / KPa	4.42	10.84	21.34	30.24
	H / kA/m	25.30	69.20	126.23	186.27
	k	3.35	6.60	10.92	15.60
	n	0.127	0.105	0.082	0.065
$\widetilde{A}_2/\widetilde{A}_4$	τ_{yAj} / KPa	5.96	20.34	37.60	45.22
	H / kA/m	38.29	116.45	244.90	427.18
	k	4.24	10.26	20.04*	34.35*
	n	0.121	0.085	0.054*	0.016*
$\widetilde{A}_3$	τ_{yAj} / KPa	4.96	14.39	28.97	41.74
	H / kA/m	26.92	83.94	179.88	318.09
	k	3.40	7.75	15.09	25.91*
	n	0.126	0.097	0.067	0.038*

Note: * marked value is estimated by extrapolating the fitting curve of fluid parameters with magnetic field according to reference [16].

According to the equation (14), the relationship of the designed MR device's torque with the shaft rotate speed when the current is 0.5 A, 1.0 A, 1.5 A and 2.0 A as shown in Fig.9 (a)~(d), respectively. With the increase of current, the shear thinning of MR fluid is intensified due to the changes of flow parameters k and n, which can also be reflected by the decrease of slope of torque curve in the post-yield. Since the magnetic field strength in the $\widetilde{A}_2$ and $\widetilde{A}_4$ effective annular shear regions is the strongest, the torque provided by these regions also accounts for the largest proportion of the total torque T_{total}, and this

proportion is more significant with the increase of current. In the case that the current is 1.0 A and the rotation speed is 3000 r/min, the sum of torque provided by $\widetilde{A}_2$ and $\widetilde{A}_4$ regions is 0.098 N.m, accounting for 52.63% of the total torque T_{total} of 0.186 N.m. The torque generated by A_1 and A_5 regions is 0.052 N.m, accounting for 28.06% of the total torque T_{total}.

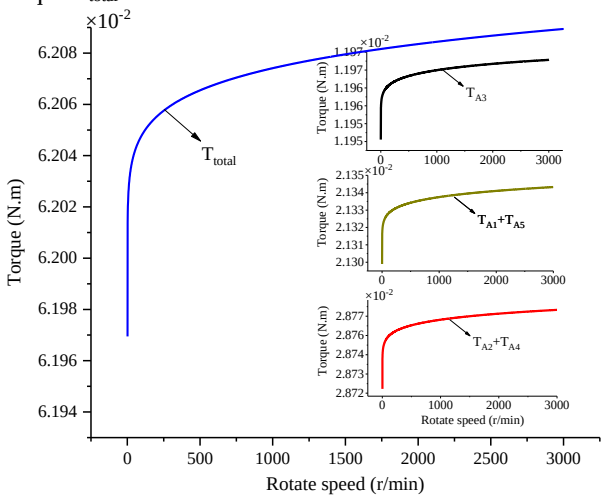

(a) I=0.5 A

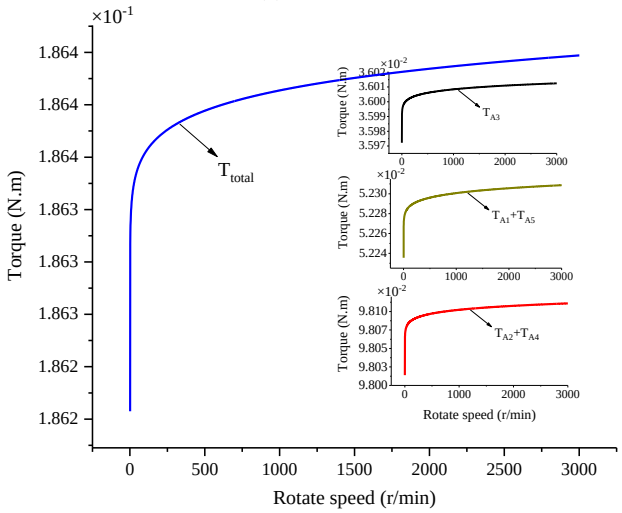

(b) I=1.0 A

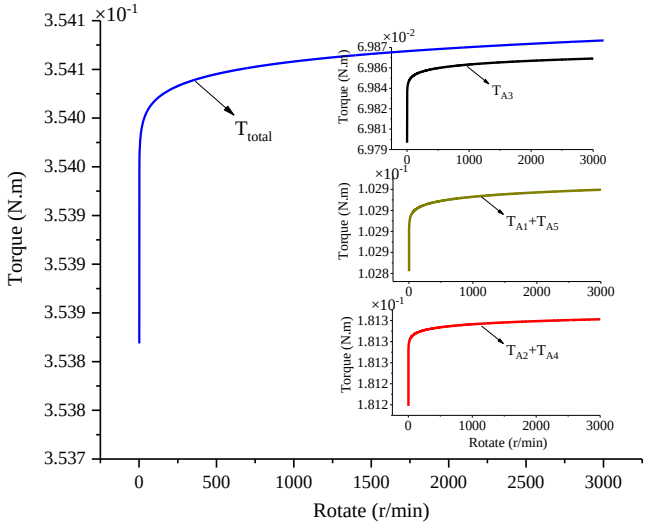

(c) I=1.5 A

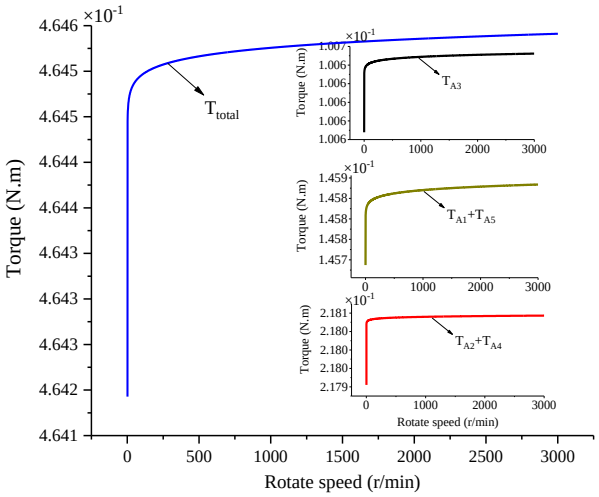

(d) I=2.0 A

Figure 9. Relationship of MR device's theoretical torque with the rotation speed

It can be seen from Figure 9 that, under 0.5 A ~ 2.0 A four different currents, the theoretical torque results are basically positively correlated with the current. However, when the current is switched from 0 A to 0.5 A, the theoretical torque calculated based on the fluid parameter value of reference [16] is not as obvious as expected, and larger torque is output when I= 1.0 A, 1.5 A and 2.0 A. This deviation, on one hand, comes from the theoretical torque calculation model, which assumes the universality of flow parameters *k* and *n* changing with the magnetic field, and without considering the influence factors of different experimental conditions and device structures. On the other hand, the defect of the device structure, which affects the stable torque value of the device output.

6. Conclusion

Through the torque analysis of the MR device, it can be seen that the consistency parameter *k* and the flow behavior index *n* of the MR fluid have significant influences on the macroscopic torque performance of MR device. The total torque of the MR device is mainly provided by the coulomb torque from the effective annular shear region, and the viscous torque from the viscous annular shear region. Due to the different magnetic field strength in each region of the fluid channel, the fluid parameters are not identical, which leads to the complexity of the torque model to some extent.

The theoretical torque are deviated at different currents and rotate speeds, especially in the case of low currents and speeds, which is mainly due to the mismatching of model parameters and the limitations of the structural design of MR device. In order to improve the stability of the output torque of the device, the structure of the device needs to be optimized in the follow-up work, such as optimizing the design of the liquid seal parts, to ensure that the MR fluid will not infiltrate into the rolling bearing, and designing the positioning parts to ensure assembly alignment.

Acknowledgment

This work was supported in part by the Natural Science Foundation of China (NSFC) Grant funded by Chinese Government under Grant 51805209, and the Key SRT project funded by the Jiaxing University under Grant CD8517193007, and in part by the National College Students' Innovation and Entrepreneurship Training Program of China under Grant 201910354013.

References

[1] Dong, S.; Lu, K.Q.; Sun, J.Q.; Rudolph, K. A prototype rehabilitation device with variable resistance and joint motion control. *Medical Engineering and Physics* **2006**, Volume 28, pp. 348-355.

[2] Gudmundsson, K.H.; Jonsdottir, F.; Thorsteinsson, F. A geometrical optimization of a magneto-rheological rotary brake in a prosthetic knee. *Smart Materials and Structures* **2010**, Volume 19, pp. 035023.

[3] Wang, D.M.; Hou, Y.F.; Tian, Z.Z. A novel high-torque magnetorheological brake with a water cooling method for heat dissipation. *Smart Materials and Structures* **2013**, Volume 22, pp. 025019.

[4] Wang, D.M.; Zi, B.; Zeng, Y.S.; Qian, S.; Qian, J. Simulation and experiment on transient temperature field of a magnetorheological clutch for vehicle application. *Smart Materials and Structures* **2017**, Volume 26, pp. 095020.

[5] Zu, Q.H.; Chen, Z.Y.; Shi, W.K.; Mao, Y.; Chen, Z.Y. Torsional vibration semiactive control of drivetrain based on magnetorheological fluid dual mass flywheel. *Mathematical Problems in Engineering* **2015**, Volume 2015, pp. 1-17.

[6] Abouobaia, E.; Bhat, R.; Sedaghati, R. Semi-active control of torsional vibrations using a new hybrid torsional damper, *European Journal of Pharmacology* **2015**, Volume 19, pp.191-198.

[7] Yu, J.Q.; Dong, X.M.; Zhang, Z.L. A novel model of magnetorheological damper with hysteresis division. *Smart Materials and Structures* **2017**, Volume 26, pp. 105042.

[8] Powers, B.E.; Wereley, N.M.; Choi, Y.T. Analysis of impact loads in a magnetorheological energy absorber using a Bingham plastic model with refined minor loss factors accounting for turbulent transition. *Meccanica* **2016**, Volume 51, pp. 3043-3054.

[9] Imaduddin, F.; Mazlan, S.A.; Zamzuri, H. A design and modelling review of rotary magnetorheological damper. *Materials and Design* **2013**, Volume 51, pp.575-591.

[10] Goncalves, F.D.; Ahmadian, M.; Carlson, J.D. Behavior of MR fluids at high velocities and high shear rates. *International Journal of Modern Physics B* **2005**, Volume 19, pp. 1395-1401.

[11] Farjoud, A.; Vahdati, N.; Yap Fook, F. Mathematical model of drum-type MR brakes using Herschel–Bulkley shear model. *Journal of Intelligent Material Systems and Structures* **2008**, Volume 19, pp. 565-572.

[12] Nguyen, Q.H.; Lang, V.T.; Choi, S.B. Optimal design and selection of magneto-rheological brake types based on braking torque and mass. *Smart Materials and Structures* **2015**, Volume 24, pp. 067001.

[13] Hung, N.Q.; Bok, C.S. Optimal design of a T-Shaped drum-type brake for motorcycle utilizing magnetorheological fluid. *Mechanics Based Design of Structures and Machines* **2012**, Volume 40, pp.153-162.

[14] Huang, J.; Yang, Y.; Huang, Y. Flow of the magnetorheological fluid in disc-type clutch. *Advanced Materials Research* **2013**, Volume 740, pp. 709-714.

[15] Assadsangabi, B.; Daneshmand, F.; Vahdati, N.; Eghtesad, M.; Bazargan-lari, Y. Optimization and design of disk-type MR brakes. *International Journal of Automotive Technology* **2011**, Volume 12, pp. 921-932.

[16] Becnel, A.; Hu, W.; Wereley, N.M. Measurement of magnetorheological fluid properties at shear rates of up to 25000 s-1. *IEEE Transactions on Magnetics* **2012**, Volume 48, pp. 3525-3528.

[17] Zheng, J.J.; Wang, X.J.; Ouyang, Q.; Li, Y.C.; Wang, J. Modeling and characterization of novel magnetorheological (MR) cell with individual currents. *Journal of Central South University* **2015,** Volume 22, pp. 2557-2567.

[18] Choi, Y.T.; Cho, J.U.; Choi, S.B.; Wereley, N.M. Constitutive models of electrorheological and magnetorheological fluids using viscometers. *Smart Materials and Structures* **2005**, Volume 14, pp.1025.

[19] Mooney, M. Explicit formulas for slip and fluidity. *Journal of Rheology* **2005**, Volume 2, pp. 210.